J|A|C|S
ARTICLES

Surface Chirality of CuO Thin Films

Roland Widmer,* Franz-Josef Haug,† Pascal Ruffieux, Oliver Gröning,
Michael Bielmann,‡ Pierangelo Gröning, and Roman Fasel

Contribution from Empa, Swiss Federal Laboratories for Materials Testing and Research,
nanotech@surfaces Laboratory, Feuerwerkerstrasse 39, CH-3602 Thun, Switzerland

Received June 9, 2006; E-mail: roland.widmer@empa.ch

Abstract: We present X-ray photoelectron spectroscopy (XPS) and X-ray photoelectron diffraction (XPD) investigations of CuO thin films electrochemically deposited on an Au(001) single-crystal surface from a solution containing chiral tartaric acid (TA). The presence of *enantiopure* TA in the deposition process results in a homochiral CuO surface, as revealed by XPD. On the other hand, XPD patterns of films deposited with *racemic* tartaric acid or the "*achiral*" *meso*-tartaric acid are completely symmetric. A detailed analysis of the experimental data using single scattering cluster calculations reveals that the films grown with L(+)-TA exhibit a CuO(1$\bar{1}\bar{1}$) orientation, whereas growth in the presence of D(−)-TA results in a CuO($\bar{1}$11) surface orientation. A simple bulk-truncated model structure with two terminating oxygen layers reproduces the experimental XPD data. Deposition with alternating enantiomers of tartaric acid leads to CuO films of alternating chirality. Enantiospecifity of the chiral CuO surfaces is demonstrated by further deposition of CuO from a solution containing *racemic* tartaric acid. The predeposited homochiral films exhibit selectivity toward the same enantiomeric deposition pathway.

Introduction

Selectivity in nature is mostly guided by chirality, in the way that many biomolecules are chiral and only one enantiomer is physiologically active. Because the other enantiomer is either inactive or even toxic, there is an increasing demand for enantioselective synthesis pathways, purification processes, and sensors. Compared to homogeneous catalysts or enzymes where the reactant and the catalyst are in the same phase (mostly liquid), heterogeneous catalysts offer a broader spectrum of application because of their activity, robustness, easier separation processes, and the possibility of reuse. Chiral surfaces have been obtained by using high-index vicinal single crystals[1−7] or by adsorbing chiral molecules on "achiral" substrate surfaces.[8−12] Recently, Switzer and co-workers[13−18] reported on the formation of chiral CuO films through electrodeposition in a solution-based process. The chirality of the deposited film on an "achiral" gold surface was defined by the type of enantiomer of the chiral tartrate ion present in the solution. During subsequent electrochemical oxidation reactions, the CuO film exhibited an enantiospecifity according to the chirality of the tartrate ion.

Such a transfer of chiral information from an organic molecule to an inorganic solid surface is of high interest[19,20] to gain deeper insight into the mechanisms of biomineralization[21−25] and stereoselective heterogeneous catalysis.[26−28]

Switzer et al. used X-ray diffraction (XRD), a bulk sensitive method, and electrochemical measurements, which are surface sensitive, to investigate the deposited CuO films. Therefore they used mostly films with a thickness of more than 400 nm. We

---

† Present address: Institut de Microtechnique, University of Neuchâtel, Breguet 2, CH-2000 Neuchâtel, Switzerland.

‡ Present address: Physics Department, University of Fribourg, Pérolles, CH-1700 Fribourg, Switzerland.

(1) McFadden, C. F.; Cremer, P. S.; Gellman, A. J. *Langmuir* **1996**, *12*, 2483.
(2) Horvath, J. D.; Gellman, A. J. *J. Am. Chem. Soc.* **2001**, *123*, 7953.
(3) Horvath, J. D.; Gellman, A. J. *J. Am. Chem. Soc.* **2002**, *124*, 2384.
(4) Ahmadi, A.; Attard, G.; Feliu, J.; Rodes, A. *Langmuir* **1999**, *15*, 2420.
(5) Attard, G. A.; Ahmadi, A.; Feliu, J.; Rodes, A.; Herrero, E.; Blais, S.; Jerkiewicz, G. J. *Phys. Chem. B* **1999**, *103*, 1381.
(6) Attard, G. A. *J. Phys. Chem. B* **2001**, *105*, 3158.
(7) Sholl, D. S.; Asthagiri, A.; Power, T. D. *J. Phys. Chem. B* **2001**, *105*, 4771.
(8) Lorenzo, M. O.; Baddeley, C. J.; Muryn, C.; Raval, R. *Nature* **2000**, *404*, 376.
(9) Humblot, V.; Haq, S.; Muryn, C.; Hofer, W. A.; Raval, R. *J. Am. Chem. Soc.* **2002**, *124*, 503.
(10) Kühnle, A.; Linderoth, T. R.; Hammer, B.; Besenbacher, F. *Nature* **2002**, *415*, 891.
(11) Fasel, R.; Parschau, M.; Ernst, K.-H. *Nature* **2006**, *439*, 449.
(12) LeBlond, C.; Wang, J.; Liu, J.; Andrews, A. T.; Sun, Y.-K. *J. Am. Chem. Soc.* **1999**, *121*, 4920.
(13) Switzer, J. A.; Kothari, H. M.; Poizot, P.; Nakanishi, S.; Bohannan, E. W. *Nature* **2003**, *425*, 490.
(14) Kothari, H. M.; Kulp, E. A.; Boonsalee, S.; Nikiforov, M. P.; Bohannan, E. W.; Poizot, P.; Nakanishi, S.; Switzer, J. A. *Chem. Mater.* **2004**, *16*, 4232.
(15) Bohannan E. W.; Kothari, H. M.; Nicic, I. M.; Switzer, J. A. *J. Am. Chem. Soc.* **2004**, *126*, 488.
(16) Poizot, P.; Hung, C.-J.; Nikiforov, M. P.; Bohannan, E. W.; Switzer, J. A. Electrochem. *Solid-State Lett.* **2003**, *6*, C21.
(17) Switzer, J. A.; Kothari, H. M.; Bohannan E. W. *J. Phys. Chem. B* **2002**, *106/16*, 4027.
(18) Oba, F.; Ernst, F.; Yu, Y.; Liu, R.; Kothari, H. M.; Switzer, J. A. *J. Ceram. Soc.* **2005**, *88*, 253.
(19) Raval, R. *Nature* **2003**, *425*, 463.
(20) Barlow, S. M.; Raval, R. *Surf. Sci. Reports* **2003**, *50*, 201.
(21) Orme, C. A. *Nature* **2001**, *411*, 775.
(22) Addadi, L.; Weiner, S. *Nature* **2001**, *411*, 753.
(23) Bouropoulos, N.; Addadi, L.; Weiner, S. *Chem. Eur. J.* **2001**, *7*, 1881.
(24) Teng, H. H.; Dove, P. M.; Orme, C. A.; De Yoreo, J. J. *Science* **1998**, *282*, 724.
(25) Cody, A. M.; Cody, R. D. *J. Cryst. Growth* **1991**, *113*, 508.
(26) *Chiral Reactions in Heterogeneous Catalysis*; Jannes, G., Dubois, V., Eds.; Plenum: New York, 1995.
(27) Blaser, H. U. *Tetrahedron: Asymmetry* **1991**, *2*, 843.
(28) Baiker, A.; Blaser H. U. In *Handbook of Heterogeneous Catalysis*; Ertl, G., Knözinger, H., Weitkamp, J., Eds.; VCH: Weinheim 1997; Vol. 5, 2422.

10.1021/ja0640703 CCC: $33.50 © 2006 American Chemical Society

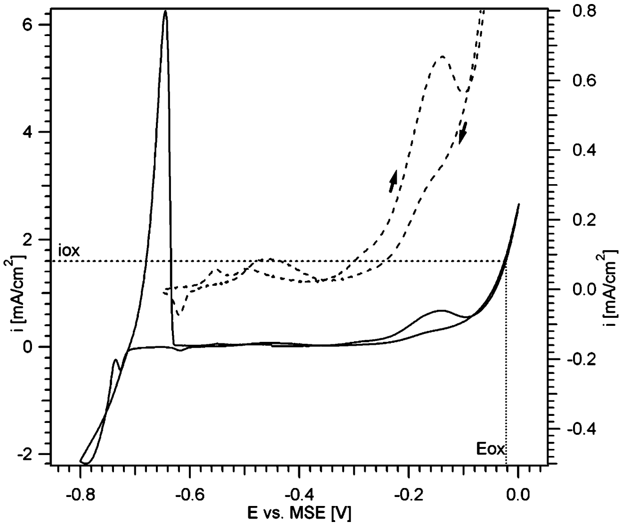

Figure 1. Cyclic voltammogramm of Au(001) in 0.2 M D(−)-TA + 0.2 M $CuSO_4$ in 3 M NaOH with a sweep rate of 10 mV/s. Deposition and dissolution of Cu_2O at the Au(001) electrode in the cathodic region, and oxidation of TA and deposition of CuO in the anodic region are observed. The dashed inset represents a zoom in (belongs to right vertical axis) and shows the monolayer adsorption/desorption of Cu on Au(001).

have performed X-ray photoelectron diffraction (XPD) experiments combined with single scattering cluster (SSC) calculations to gain more insight into the properties of the topmost surface layers and selectivity at the surface, and to understand the nucleation and growth at molecular and atomic level.

Experimental Section

All deposition experiments were performed in solutions of reagent grade chemicals: 0.2 M tartaric acid (TA), 0.2 M $CuSO_4 \cdot 5H_2O$, and 3 M NaOH in ultrapure water (18.2 MΩ, ELGA). The substrates, commercial Au(001) single crystals (MaTecK GmbH) with an orientation better than 0.4°, were mechanically polished with diamond paste down to 0.1 μm, cleaned, and annealed with a hydrogen flame under N_2-flux just before the experiments. Electrochemical deposition of the CuO films was performed with an Autolab PGSTAT30 in a conventional three-electrode cell with a saturated mercury sulfate (MSE) reference electrode and a glassy carbon counter electrode. The CuO films were deposited galvanostatically with an anodic current density of 1.6 mA/cm^2 at a potential of −20 mV vs MSE according to the cyclic voltammogram shown in Figure 1. In the cathodic region Cu_2O bulk deposition occurs after the adsorption of a monolayer, while in the anodic region with the oxidation peak of the TA, the CuO deposition starts at about $E > -250$ mV vs MSE. Films with a thickness ranging from 1 to 150 nm (determined by scanning force microscopy and correlated with the charge density) were grown using L(+)-, D(−)-,DL-, and *meso*-TA in the electrolyte.

After thoroughly rinsing the deposited CuO films with ultrapure water, they were transferred into ultrahigh-vacuum and analyzed in an Omicron ESCA XPS/XPD system. The base pressure of the system is 5×10^{-11} mbar, and an Al Kα X-ray tube (1486.6 eV) was used as photon source. XPD patterns were measured over a large part of the hemisphere above the sample surface: Core-level photoelectron intensities were collected on a dense grid of polar emission angles (θ) from normal emission (0°) to 70° and over the full 360° azimuthal angle (φ) range. The XPD patterns are represented in a stereographic projection of the scattered photoelectron intensity in real space. The outer ring delimiting the XPD patterns indicates a polar emission angle of 90°, i.e., emission along the surface plane, and the center of the patterns corresponds to emission along the surface normal. The photoelectron intensity is given in a linear gray scale representation, with white corresponding to maximum intensity. To enhance the statistical accuracy, the data shown have been azimuthally averaged according to the 4-fold rotational symmetry of the Au(001) substrate surface. Model calculations to simulate the XPD patterns were performed using the SSC model[29] for bulk-truncated CuO structures. In combination with the chemically sensitive XPD, which has proven to be a powerful tool for structural investigations of the near-surface region,[30] the SSC calculations allow one to get insight into structural aspects of thin layers and, in particular, their surface termination.

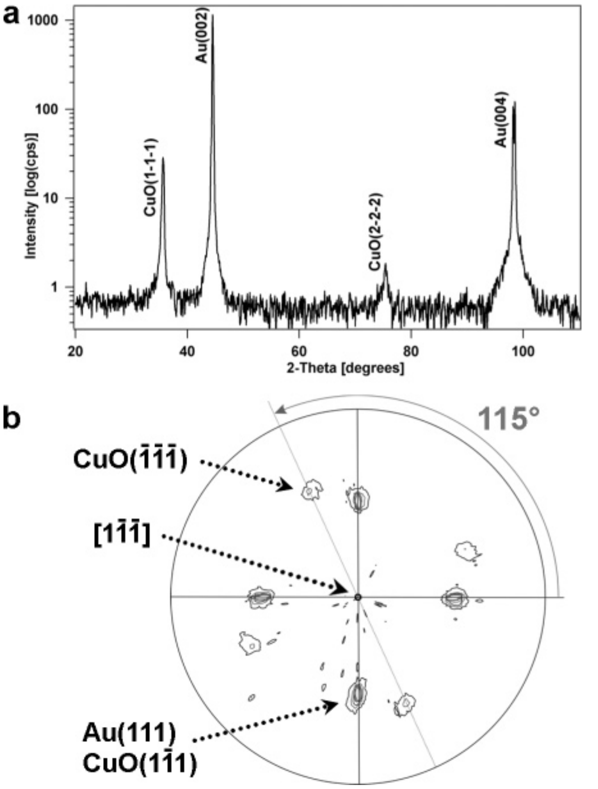

Figure 2. (a) XRD data of 125 nm CuO electrodeposited in the presence of L(+)-TA onto a single-crystal Au(001) surface. (b) Cu Kα_1 X-ray pole figure determination of the absolute configuration of chiral CuO deposited in the presence of L(+)-TA, indicating that the system has a CuO($1\bar{1}\bar{1}$)//Au(001) epitaxial relationship.

To connect to the previous experiments by Switzer,[13,14] the bulk crystallographic properties of epitaxial films were characterized by XRD in $\theta-2\theta$ configuration and by pole figure measurements with a Siemens D5000 diffractometer using Cu Kα_1 radiation.

Results and Discussion

In the bulk analysis, our films exhibit the same XRD data as reported by Switzer et al.,[13,14] with prominent $(1\bar{1}\bar{1})$ and $(2\bar{2}\bar{2})$ peaks of the CuO planes and the (002) and (004) peaks of the underlying Au substrate, as shown in Figure 2a for a 125 nm thick CuO film deposited in the presence of L(+)-TA. The X-ray pole figure (Figure 2b) was measured at a Bragg angle of 38.4°, which probes the planes of Au(111). Due to their nearly identical *d* spacing, additional contributions of the $(\bar{1}1\bar{1})$ and (111) planes of CuO are expected. Diffraction at (002) planes of CuO may also occur but shows lower intensity, as is expected for a higher 2θ angle.

---

(29) Fadley C. S. In *Synchrotron Radiation Research: Advances in Surface and Interface Science, Vol. 1: Techniques*; Bachrach, R. R. Z., Ed.; Plenum Press: New York, 1992; 421 and references therein.

(30) Fasel, R.; Aebi, P. *Chimia* **2002**, *56*, 566. Westphal, C. *Surf. Sci. Rep.* **2003**, *50*, 1. Osterwalder, J.; Aebi, P.; Fasel, R.; Naumovic, D.; Schwaller, P.; Kreutz, T.; Schlapbach, L.; Abukawa, T.; Kono, S. *Surf. Sci.* **1995**, *331−333*, 1002.

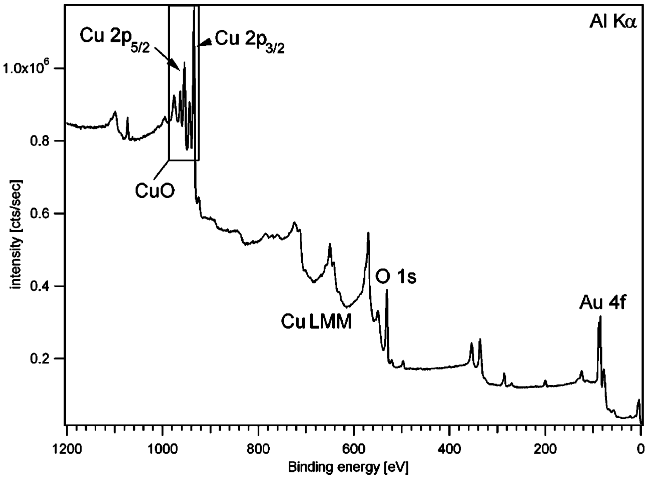

Figure 3. XPS spectrum of a 30 nm thin CuO film on a Au(001) substrate, with the typical CuO multiplet structure highlighted. XPD experiments were performed with the peaks labeled Cu $2p_{3/2}$, Cu LMM (Auger), O 1s, and Au 4f.

The pole figure of Figure 2b shows the (111) poles of the gold substrate at a tilt angle of $\chi = 55°$, superimposed with four rotationally equivalent $(1\bar{1}1)$ poles of the epitaxial CuO film. Four corresponding CuO$(\bar{1}\bar{1}\bar{1})$ poles are observed for a sample tilt of $\chi = 63°$ and rotated counterclockwise by 115° with respect to the Au(111) and CuO$(1\bar{1}1)$ poles.

A film with $(\bar{1}11)$ orientation would result in the same $\theta{-}2\theta$ diffractogram due to the identical plane spacings, but in the pole figure the corresponding (111) poles at $\chi = 63°$ would be rotated clockwise by 115°. The absence of these poles in the figure suggests growth of a purely $(1\bar{1}\bar{1})$ oriented CuO film on the Au(001) surface. Pole figures of the CuO$(1\bar{1}\bar{1})$ and the CuO-$(\bar{1}11)$ films are non-superimposable mirror images that cannot be transferred into each other by rotation and translation, which indicates that the two films are enantiomers.

As chiral recognition and selectivity take place at the very surface of a catalyst, we have applied photoelectron spectroscopic methods in order to obtain information about surface orientation and termination. The surface sensitivity of these methods is due to a limited mean-free path of the photoelectrons in the substrate, which is of the order of 1.2 nm for the photoelectron energies used in our XPD study.[31] The typical multiplet pattern of the Cu 2p peaks in the XPS spectra (Figure 3) confirms the deposition of a CuO thin film. Compared to other samples transferred through air, only a weak carbon peak is discernible in the spectra, indicating a relatively inert surface. In all XPD experiments the Cu $2p_{3/2}$, Cu LMM (Auger peak), O 1s, and the Au $4f_{7/2}$ peaks were measured. The Au 4f reference peak decreases in intensity for thicker CuO films but is discernible even for 125 nm thick films. This is due to the particular hatlike shape of the Au(001) crystal, which avoids the CuO film to cover the entire gold surface. The CuO was deposited using the meniscus technique, where only the forefront surface of the hatlike shaped crystal was exposed to the electrolyte.

Figure 4 shows the Au 4f XPD pattern of the clean Au(001) surface (Figure 4a), which allows one to determine the orientation of the substrate, and the Cu 2p XPD patterns of 30 nm thick films deposited with L(+)-TA (Figure 4c) and D(−)-TA (Figure 4d). The Cu 2p XPD patterns of films grown with either L(+)- or D(−)-TA (Figure 4c,d) are clearly non-superimposable mirror images of each other, indicating that the two film surfaces are enantiomers. The chirality can be revealed by attributing a windmill-like rotational direction with the bright feature labeled A, at about $\theta = 40°$, the intensity distribution within the triangular feature labeled B at about $\theta = 55°$, and the three-feature group labeled C at $\theta = 70°$, which point out the above-mentioned non-superimposable mirror images. The experimentally obtained Cu 2p XPD patterns of the CuO films deposited with L(+)- and D(−)-TA (Figure 4c,d) are compared with those obtained by SSC calculations (Figure 4e,f). Despite the simplicity of the SSC model, the calculated XPD patterns exhibit a good agreement of the single features, the overall appearance

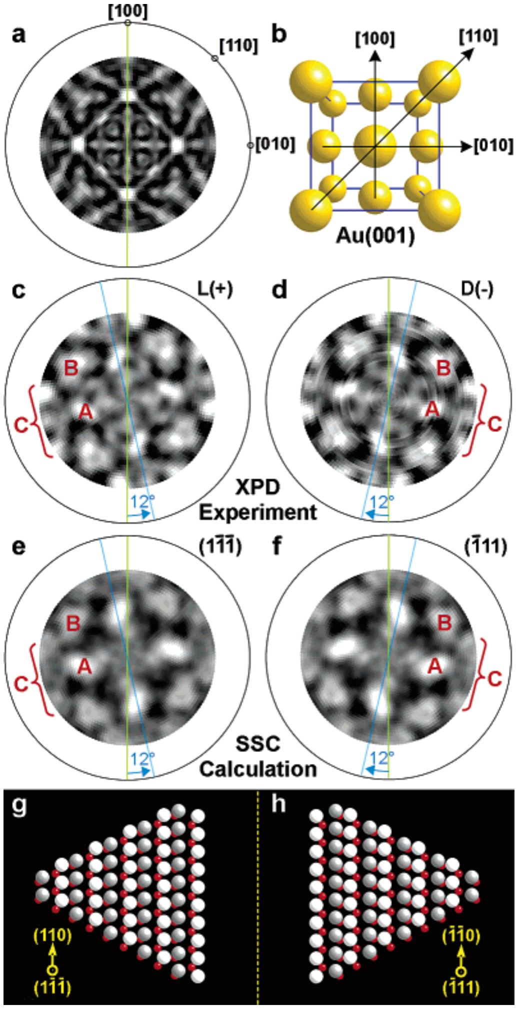

Figure 4. XPD patterns with a green line for the orientation of the Au(001) substrate and a blue line for the position of a selected CuO peak. The patterns were measured from 0 to 70°, and the outer circle denotes a polar emission angle of 90°. (a) The Au 4f XPD pattern, allowing one to determine the orientation of the substrate surface as indicated by some high-symmetry directions. (b) Au(001) unit cell with directions according to a. (c) Cu $2p_{3/2}$ XPD pattern of a 30 nm CuO film electrodeposited in the presence of L(+)-TA. A, B, and C indicate prominent features at $\theta = 40$, 55, and 70°. (d) Cu $2p_{3/2}$ XPD pattern of a 30 nm CuO film electrodeposited in the presence of D(−)-TA. (e) Cu $2p_{3/2}$ SSC calculation for an O_{II}-terminated CuO$(1\bar{1}\bar{1})$ surface. (f) Cu $2p_{3/2}$ SSC calculations for an O_{II}-terminated CuO$(\bar{1}11)$ surface. (g, h) Model representations of the CuO $(1\bar{1}\bar{1})$ and $(\bar{1}11)$ surfaces, with red for Cu atoms, white for the O atoms closest to the Cu plane sitting in 3-fold hollow sites (O_I), and gray for the O atoms nearly atop the Cu atoms (O_{II}).

---

[31] National Institute of Standards and Technology. *Standard Reference Database 71*, Version 1.1; 2000.

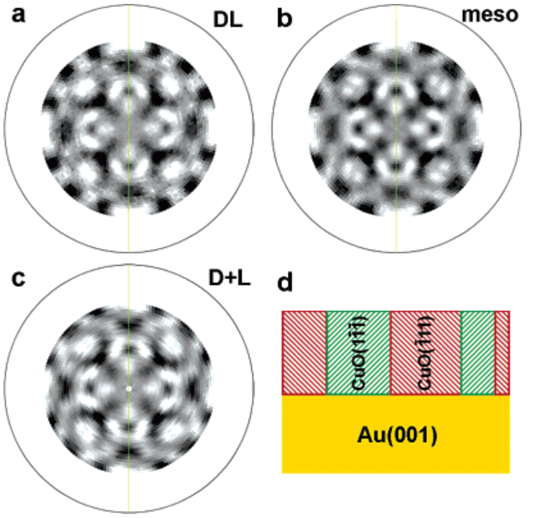

Figure 5. (a) Cu $2p_{3/2}$ XPD pattern of a 30 nm CuO film electrodeposited in the presence of racemic DL-TA. (b) Cu $2p_{3/2}$ XPD pattern of a 30 nm CuO film electrodeposited in the presence of “achiral” *meso*-TA. (c) Mathematical superposition of the Cu $2p_{3/2}$ XPD patterns measured for CuO films deposited from L(+)- and D(−)-TA solutions, respectively, which are given in Figure 4c,d. (d) Schematic representation of the film morphology obtained by electrodeposition from the racemic DL-TA solution.

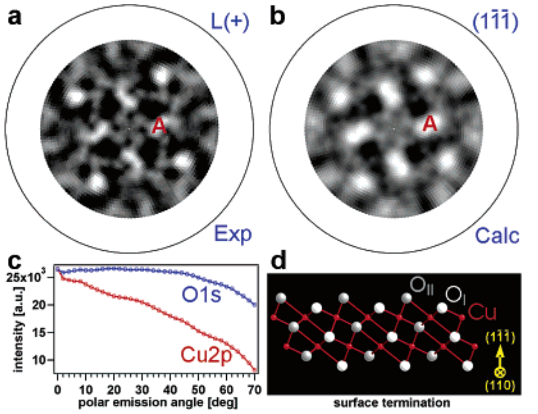

Figure 6. (a) O 1s XPD pattern of a 30 nm CuO film electrodeposited in the presence of L(+)-TA, with indication A for the feature at $\theta = 40°$. (b) O 1s SSC calculation for an O_{II}-terminated CuO$(1\bar{1}\bar{1})$ surface. (c) Cu $2p_{3/2}$ (red) and O1s (blue) intensity profiles for polar emission angles from normal emission (0°) to grazing emission (70°). (d) Side view of a bulk-truncated CuO film with O_{II}-termination and $(1\bar{1}\bar{1})$ surface orientation, which is obtained for CuO deposition with L(+)-TA.

and orientation. From the SSC calculations the surface orientation of the CuO thin films can be unambiguously determined to be $(1\bar{1}\bar{1})$ for the deposition in the presence of L(+)-TA, and $(\bar{1}11)$ for the deposition in the presence of D(−)-TA. The green vertical line drawn in the XPD plots represents the orientation of the Au(001) substrate, whereas the blue line indicates the orientation of a selected feature of the CuO films. In comparison with the orientation of the substrate a rotation of 12° counterclockwise for films deposited with L(+)-TA, and of 12° clockwise for films deposited with D(−)-TA is observed. Parts g and h of Figure 4 show model representations of the resulting CuO films with $(1\bar{1}\bar{1})$ and $(\bar{1}11)$ surfaces for deposits with L-(+)- and D(−)-TA, respectively, demonstrating the CuO[110]//Au[110] epitaxial relationship. Because there are two inequivalent O atoms, they are colored white for the atoms closest to the Cu plane sitting in 3-fold hollow sites (O_I) and gray for the O atoms nearly atop the Cu atoms (O_{II}).

Figure 5 summarizes investigations of the CuO film growth from solutions containing racemic mixtures (DL) of L(+)- and D(−)-TA or the “achiral” *meso*-TA. CuO films grown from racemic DL-TA and from *meso*-TA exhibit achiral, symmetric XPD patterns, as can clearly be seen in Figure 5a,b, respectively. For comparison, Figure 5c shows an XPD pattern obtained by mathematical superposition of the experimental patterns from enantiopure L(+)- and D(−)-TA grown CuO films (Figure 4c,d). The comparison with Figure 5a,b shows that this mathematical superposition reproduces the XPD patterns measured from DL-TA and *meso*-TA deposited CuO films perfectly well. This strongly suggests that the DL-TA and *meso*-TA deposited CuO films consist of equal amounts of the two enantiomeric orientations (domains) and thus appear completely symmetric. The XPD pattern from the film deposited with the achiral *meso*-TA (Figure 5b), which is the achiral analogue to the tartaric acid, exhibits a slightly higher anisotropy than the racemic one (Figure 5a). This can be rationalized by the growth of somewhat larger homochiral domains in the case of *meso*-TA. Due to the propensity of *meso*-TA to distort into either a pseudo L(+)- or D(−)-TA conformation,[32] the CuO film can grow in both orientations, but according to a two-dimensional analogue of the “sergeants and soldiers” mechanism,[33] the growth might be largely driven by the initial orientation of the nucleation site, and laterally continued until the growing domain collides with another domain growing from the next nucleation site. In the presence of racemic DL-TA, on the other hand, the probability of changing domain orientation during film growth is higher since there are two determined enantiomeric species that each only allow growth with one distinct orientation.

As mentioned above, the handedness of the very surface as well as the chemical identity of the surface termination play an important role for chiral recognition and catalytic activity. Figure 6a displays the O 1s XPD pattern, which exhibits again a chiral orientation and is compared with a SSC calculation in Figure 6b. As before a very good agreement between the experimental data and the SSC calculations is obtained. From a detailed investigation of the different possible surface terminations (Cu-terminated, O_I-terminated, O_{II}-terminated, see Figure 6d), including an analysis of the O 1s intensity distribution and comparison with the position of diffraction features in the SSC calculations, it can be concluded that the surface is O_{II}-terminated. For further affirmation, the experimental O 1s and Cu 2p intensity distributions were azimuthally averaged and normalized to each other at normal emission, yielding the polar-angle-dependent intensity distributions shown in Figure 6c. It is apparent that the intensity of the O 1s signal is always above the one of the Cu 2p, and its slope decreases less with higher θ-angles. This also confirms an O-termination of the surface, which is certainly not unexpected given that the CuO films are grown in an oxidizing process. Figure 6d displays the corresponding model structure of the O_{II}-terminated CuO surface, with the appropriate $(1\bar{1}\bar{1})$ orientation for a deposition with L-(+)-TA. Since catalytic reactions or deposition processes are mainly influenced by the surface termination, it is the chiral arrangement of the topmost oxygen atoms with respect to the underlying copper layer that is responsible for the enantioselectivity of the CuO films.

---

(32) Parschau, M.; Kampen, T.; Ernst, K. H. *Chem. Phys. Lett.* **2005**, *407*, 433.
(33) Green, M. M.; Reidy, M. P. *J. Am. Chem. Soc.* **1989**, *111*, 6452.

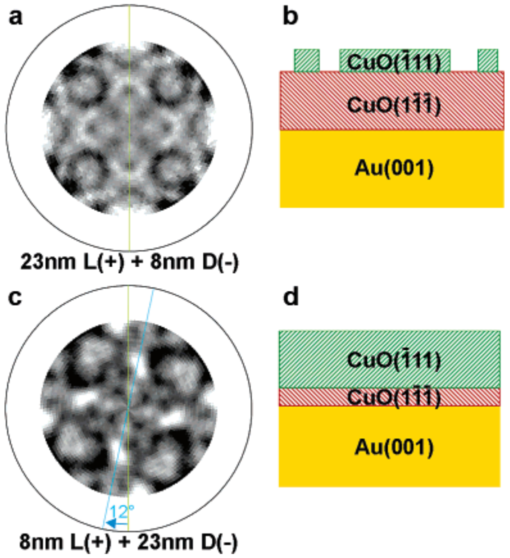

Figure 7. Cu $2p_{3/2}$ XPD patterns of CuO films with alternating chirality. The green line indicates the [100] orientation of the underlying Au(001) substrate. (a) CuO film electrodeposited first in the presence of L(+)-TA to a thickness of 23 nm, with subsequent deposition of 8 nm CuO in the presence of D(−)-TA. (b) Schematic representation of the film formation according to the XPD pattern from a. (c) CuO film electrodeposited first in the presence of L(+)-TA to a thickness of 8 nm, with subsequent deposition of 23 nm CuO in the presence of D(−)-TA. (d). Schematic representation of the film formation according to the XPD pattern from c.

In a next step, we investigated whether it was possible to grow CuO films with alternating chirality, which would be interesting for applications in nonlinear optics. “Double-decker” films were produced by first depositing a certain thickness of CuO using one enantiomer, followed by further film growth using the opposite enantiomer. Between the deposition cycles the sample was thoroughly rinsed with ultrapure water. To prevent emission of photoelectrons from the underlying CuO film to contribute to the XPD patterns, a minimum thickness of 8 nm was chosen for the second growth step. Figure 7a shows the Cu 2p XPD pattern of a film where the first 23 nm was deposited with L(+)-TA, and then 8 nm with D(−)-TA on top. The XPD pattern appears completely symmetric and compares well to the patterns shown in Figure 5. This indicates that the growth mechanism has changed the orientation of the film in the second deposition step but that 8 nm is not yet enough to completely invert the growth orientation. This is a strong indication for nucleation of a film with the inverse chirality on top of the predeposited CuO film, as sketched in Figure 7b.

A complete reversal of chirality is observed for the inverse deposition sequence, that is a first deposition of 8 nm with L(+)-TA followed by a 23 nm deposition with D(−)-TA. The XPD pattern resulting from this 8 nm L / 23 nm D film is given in Figure 7c. Exactly as in Figure 4d, a rotation of 12° clockwise is seen, and the shape and position of peaks correspond perfectly well to those of a film deposited with D(−)-TA only. This proves that 23 nm further deposition with the opposite enantiomer is sufficient to completely invert the pattern, and thus the handedness of the film. The initially deposited film thus gets overgrown by a closed film with the opposite orientation, as schematically shown in Figure 7d. This process can in principle be continued for many more layers, resulting in the formation of a multilayer film with alternating chirality.

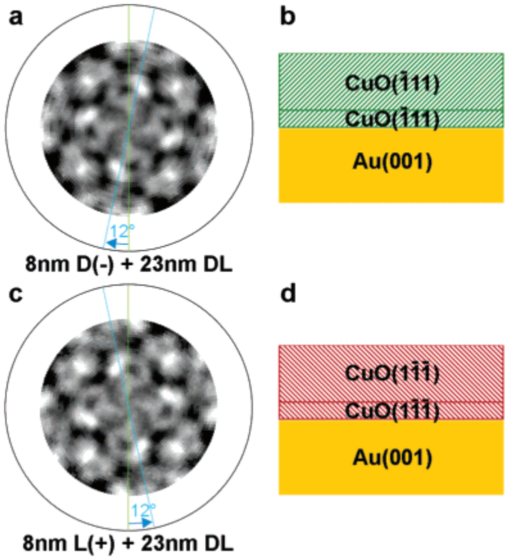

Figure 8. XPD investigation of the chiral CuO surfaces with respect to enantioselective growth continuation. The green line indicates the [100] orientation of the underlying Au(001) substrate, and the blue line the position of the feature A of the Cu $2p_{3/2}$ XPD patterns. (a) CuO film electrodeposited first in the presence of D(−)-TA to a thickness of 8 nm, with subsequent deposition of 23 nm CuO in the presence of racemic DL-TA. (b) Schematic representation of the film formation according to the XPD pattern from a. (c) CuO film electrodeposited first in the presence of L(+)-TA to a thickness of 8 nm, with subsequent deposition of 23 nm CuO in the presence of racemic DL-TA. (d) Schematic representation of the film formation according to the XPD pattern from c.

So far, we have seen that (i) CuO deposition from enantiopure D(−)- or L(+)-TA solutions results in homochiral surfaces exhibiting $(\bar{1}11)$ or $(1\bar{1}\bar{1})$ oriented surfaces, respectively, (ii) CuO deposition from racemic DL-TA results in an overall achiral surface exhibiting domains of both $(\bar{1}11)$ and $(1\bar{1}\bar{1})$ surface orientations, and (iii) that $(1\bar{1}\bar{1})$ oriented films grown with L-(+)-TA can be overgrown by $(\bar{1}11)$ oriented films using the opposite D(−)-TA. From these observations, the following question naturally arises: Does CuO deposition from a racemic DL-TA solution on top of a predeposited enantiopure $(\bar{1}11)$ or $(1\bar{1}\bar{1})$ oriented film also give rise to a racemic surface orientation? Or does the predeposited enantiopure CuO film exhibit selectivity with respect to growth continuation with the same handedness? In analogy to the enantioselective electrochemical oxidation of tartaric acid on homochiral CuO films that has been observed by Switzer and co-workers,[13−15] we expect the CuO films to exhibit chiral recognition and to selectively steer further CuO deposition toward one particular enantiomeric deposition pathway. To test this hypothesis, we have deposited CuO from a racemic DL-TA solution onto predeposited, enantiopure CuO films. Figure 8a shows the Cu 2p XPD pattern of a 8 nm CuO film deposited with D(−)-TA, followed by 23 nm deposited with the racemic DL-TA on top. It is clearly seen that the XPD pattern (Figure 8a) exhibits the same features and rotation as the one of CuO grown with enantiopure D(−)-TA (Figure 4d). The same behavior is observed for deposition of first 8 nm CuO with L-(+)-TA, followed by 23 nm with racemic DL-TA. Again, the XPD pattern of the resulting film (Figure 8b) exhibits the characteristic features of a CuO film grown with enantiopure L(+)-TA (Figure 4c). The subsequent growth on top of a predeposited D(−)- or L(+)-CuO film in the presence of racemic DL-TA thus follows the deposition pathway as for pure D(−)-

or L(+)-TA, respectively. This clearly demonstrates chiral selectivity of the homochiral CuO films: Film growth on top of a predeposited chiral CuO film continues in the particular chiral form even in the presence of racemic DL-TA. This enantioselectivity is due to a significantly higher current density in the oxidation process of one particular enantiomer on the homochiral CuO surface. During a deposition process in the presence of a racemic electrolyte onto a predeposited homochiral CuO surface, one particular Cu−TA−enantiomer complex is thus preferentially oxidized, which leads to homochiral growth continuation.

Conclusions

We have shown that the formation of chiral CuO surfaces through electrodeposition in a solution-based process is possible down to film thicknesses of a few nanometers. The properties of thicker films, as demonstrated with XRD and X-ray pole figure data, are retained also for these very thin films. A detailed analysis of XPD data reveals that the chiral CuO thin films are terminated with two oxygen layers (O_{II}-termination). CuO deposition in the presence of racemic DL-TA results in the formation of a racemic mixture of $(\bar{1}11)$ and $(1\bar{1}\bar{1})$ domain orientations. It is interesting to note that for DL-TA deposition on a Cu surface in ultrahigh vacuum, a similar formation of a racemic mixture of domain orientations has been reported.[34] Since XPD is sensitive to an area of several mm^2, single domains cannot be resolved, but the resulting XPD patterns are an average of the diffraction patterns from the two domain orientations. The same holds true for deposition in the presence of the “achiral” *meso*-TA, since the Cu-ion in the tartaric complex is known to be stabilized with one carboxyl and one alcohol group.[35] This results in a 1:1 occurrence of “pseudo D(−)”- and “pseudo L(+)”-TA conformations, and again the formation of two domains with opposite enantiomeric orientation. While CuO films deposited in the presence of DL-TA take both domain orientations, deposition in the presence of the single TA enantiomer results in a homochiral surface exhibiting a single domain orientation. Deposition from a D(−)-TA solution results in $(\bar{1}11)$-oriented CuO films, whereas L(+)-TA governs the formation of $(1\bar{1}\bar{1})$-oriented CuO films.

Deposition of 23 nm CuO in the presence of one enantiomer on top of a CuO film predeposited with the other enantiomer totally changes the appearance of the XPD pattern towards the other orientation. An oppositely oriented film can thus be grown on top of a chiral CuO film by exchange of the TA enantiomer in the solution. In this way, CuO films with alternating chirality can be grown on top of the Au(001) surface, which might be of potential technological interest for applications in nonlinear optics.

Studies of CuO growth from racemic DL-TA solution on top of a predeposited homochiral CuO film clearly demonstrate selectivity of the chiral CuO films toward growth continuation with the same film orientation: Deposition of 23 nm CuO from a DL-TA solution on top of a predeposited CuO$(\bar{1}11)$ film does not alter the film orientation, but due to enantioselectivity the growth continues with the same $(\bar{1}11)$ orientation. This is in distinct accordance with the selective electrochemical oxidation of TA demonstrated by Switzer and co-workers[13−15] and thus highlights the prominent role of the TA oxidation step in the enantioselective CuO deposition process.

With these observations we have obtained a first glimpse at the intriguing enantioselective CuO deposition mechanism. Detailed investigations of the initial CuO nucleation stage by means of electrolytic in-situ STM are under way.

Acknowledgment. We thank Karl-Heinz Ernst for stimulating discussions.

JA0640703

---

(34) Romer, S.; Behzadi, B.; Fasel, R.; Ernst, K. H. *Chemistry* **2005**, *11* (14), 4149.

(35) Missavage, R. J.; Belford, R. L.; Paul, I. C. *J. Coord. Chem.* **1972**, *2*, 145.